Journal of Neural Engineering

PAPER

The role of distinct ECoG frequency features in decoding finger movement

Eva Calvo Merino[*] (ID) , A Faes (ID) and M M Van Hulle (ID)

Laboratory for Neuro- and Psychophysiology, KU Leuven, Leuven, Belgium
[*] Author to whom any correspondence should be addressed.

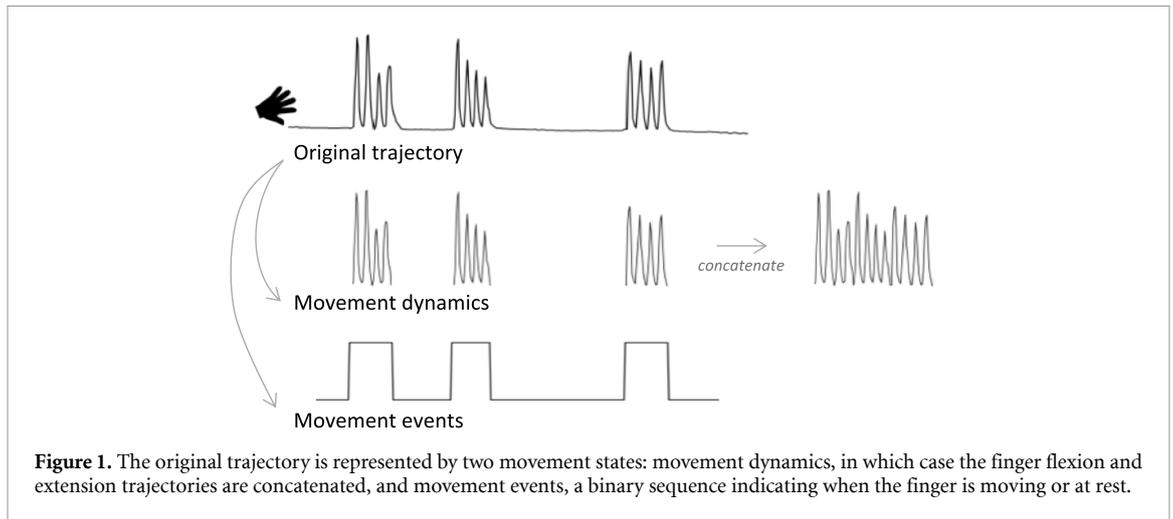**E-mail:** eva.calvomerino@kuleuven.be

Abstract

Objective. To identify the electrocorticography (ECoG) frequency features that encode distinct finger movement states during repeated finger flexions. *Approach.* We used the publicly available Stanford ECoG dataset of cue-based, repeated single finger flexions. Using linear regression, we identified the spectral features that contributed most to the encoding of movement dynamics and discriminating movement events from rest, and combined them to predict finger movement trajectories. Furthermore, we also looked into the effect of the used frequency range and the spatial distribution of the identified features. *Main results.* Two frequency features generate superior performance, each one for a different movement aspect: high gamma band activity distinguishes movement events from rest, whereas the local motor potential (LMP) codes for movement dynamics. Combining these two features in a finger movement decoder outperformed comparable prior work where the entire spectrum was used as the average correlation coefficient with the true trajectories increased from 0.45 to 0.5, both applied to the Stanford dataset, and erroneous predictions during rest were demoted. In addition, for the first time, our results show the influence of the upper cut-off frequency used to extract LMP, yielding a higher performance when this range is adjusted to the finger movement rate. *Significance.* This study shows the benefit of a detailed feature analysis prior to designing the finger movement decoder.

1. Introduction

Every year, half a million patients worldwide face paralysis due to the disruption of signal pathways between the brain and the muscles primarily due to spinal cord injury, brainstem stroke or amyotrophic lateral sclerosis [1]. The quality of life of these patients would significantly improve should they regain a degree of voluntary motor control. By translating brain commands into motor actions directly, brain computer interfaces (BCIs) can bypass defective neural pathways. This has been successfully demonstrated in patients controlling a paralysed upper limb through neuromuscular stimulation [2, 3], a prosthetic limb [4, 5] an exoskeleton [6], or having their imagined handwriting movements translated into text [7]. Despite these accomplishments, more research is needed before motor BCIs are able to support humans in their more complex motor

behaviours such as skilled finger movements [8], which they enable us to perform countless daily life actions: holding hands, grasping objects, or playing a musical instrument, to name a few.

Over the past few years, research on how to decode finger movements from brain activity has increasingly gained ground. The neural and muscular mechanisms involved in finger movements significantly differ from those controlling other limbs [8], thus requiring specific BCI solutions. Several studies have reported some level of differentiation in the brain representation of individual fingers [8, 9], which in turn has been exploited to develop decoders that either classify which finger is moving or that predict its trajectory (flexion or extension), a much harder task. Finger movement classifiers have been developed using common spatial pattern filters followed by linear models [10, 11], conditional random fields [12], and decision trees [13]. As to finger trajectory

Figure 1. The original trajectory is represented by two movement states: movement dynamics, in which case the finger flexion and extension trajectories are concatenated, and movement events, a binary sequence indicating when the finger is moving or at rest.

decoding—the focus of this work—several regression techniques have already been exploited, most of them applied to the BCI competition IV dataset to facilitate comparison [14]. In this competition, the best performance was for the linear approach of [15], with an 0.46 average Pearson correlation coefficient between predicted and actual finger trajectories [16]. In [17], deep learning was applied to the same dataset yielding a correlation coefficient of 0.515. Riemannian features together with gradient boosting trees lifted the performance up to 0.537 [18], with tensor-based methods further improving it to 0.59 [19].

Electrocorticography (ECoG) is a partially invasive recording technique commonly used to study the brain dynamics involved in finger movements [20]. Compared to other brain recording techniques, including more invasive ones such as microwires that enter the cortical tissue or non-invasive ones such as electroencephalography (EEG) and magnetoencephalography, ECoG exhibits several advantages for finger decoding. ECoG signals enjoy a wider frequency range, larger amplitude, and higher spatial resolution than their non-invasive counterparts [21]. On the other hand, unlike the more invasive techniques, ECoG electrode grids are placed on the surface of the brain thereby avoiding damage to brain vasculature and fibrous scar tissue formation that could affect long-term signal stability [20]. From a finger decoding perspective, ECoG grids should be placed over the somatomotor regions of the cerebral cortex, specifically over a brain region called the 'hand knob' area which represents the human hand [8, 22].

Current studies on finger-based BCIs tend to focus on improving decoder performance, with far less attention paid to signal features and how they relate to the information of interest. When it comes to movement, the analysis of frequency features has already suggested that different timescales hold different information. Power in lower frequency

oscillations (<30 Hz) has been linked to subcortical regions projecting to a range of cortical areas [23]. Power in higher frequencies, in contrast, is thought to represent more localized cortical processing [24], with oscillations above 60 Hz strongly correlating with average neural firing rates [25]. The instantaneous amplitude of the low frequency oscillations, called local motor potential (LMP) [26, 27], has been suggested to hold information related to motor planning and execution. Moreover, cross-frequency coupling is believed to play a key role in neural communication and cognitive processing [23, 28]. Following this, we hypothesize that adapting motor BCI systems to the specific characteristics of frequency features could help enhance finger decoding performance.

Instead of focussing on algorithm development, we first investigated the contribution of individual frequency bands to finger movement across different movement states. We distinguished two main states: movement dynamics and movement events (figure 1). We identified, using linear regression, the spectral features, and their combination, that best predict each state. Second, we applied a simple decoder, again based on linear regression, to predict finger movement trajectories based on the identified features and compare its performance to that of previous work. Finally, we analysed the contribution of the temporal and spatial characteristics of the identified features, and how our findings could be beneficial to other motor BCI paradigms.

2. Methods

2.1. Datasets
This study uses publicly available simultaneous ECoG/data glove recordings of nine subjects released

by Stanford University[2] [29]. The ECoG grids featured, depending on the subject, 38–64 electrodes of 4 mm diameter (2.3 mm exposed surface) with 1 cm inter-electrode distance. ECoG grids are routinely implanted to localize the epileptogenic zone and eloquent cortex, with the included subjects selected for their ECoG grids coverage of the hand knob area of the (pre)motor cortex. As mentioned in the introduction, much of prior research on finger movement detection relied on the BCI competition IV dataset with ECoG signals from three subjects, which are also included in the nine subject Stanford dataset we report on in this paper. We refer to these subjects with a numerical code ranging from 1 to 9. To facilitate comparison with previous studies, the correspondence between our numbering and that of the two datasets is listed in table S1. During acquisition, the brain signals were sampled at 1000 Hz and band pass filtered between 0.15 and 200 Hz. While ECoG activity was recorded, subjects were asked to perform self-paced finger movements during two-second trials, with a two-second rest period between trials. The entire experiment lasted around 10 min per subject. From an open hand starting position, subjects performed around 2–5 finger flexions per trial with each trial assigned to a specific finger in a randomized manner, indicating the finger to move with a word displayed on a bedside monitor. See table S1 for more information on the number of available trials per subject. Finger trajectories were recorded using a 5-sensor data glove the subjects wore during the experiment.

2.2. Movement states

The finger trajectories recorded by the data glove were divided into two movement states: movement dynamics and movement events (figure 1).

Movement dynamics is formed by concatenating, for each cued finger individually, all periods when the subject was purposefully moving the cued finger; instances where a non-cued finger moved were not included, as they were possibly caused by the unintentional movements of fingers adjacent to the cued one (finger co-activation [30]). Movement events are labelled per time sample by '1' when a cued finger moved, and '0' when at rest or when a finger was moved due to coactivations. To detect when a specific finger was moving we followed the strategy of [18], based on the BCI competition IV and Stanford datasets, but added an extra step in which the three time samples surrounding a detected movement period

were also labelled as '1'. This extra step was added after visually inspecting the labelled data and it allowed us to better capture the complete movement period.

2.3. Signal pre-processing

Initially, we visually inspected the ECoG signals and removed noisy channels. For some subjects, a few samples from the beginning of the recording were also removed, as they had been collected before the first finger movement. These samples were removed both from the finger trajectories and the ECoG signals (see table S1 for details).

The ECoG data was re-referenced to the common average, and notch filters were applied to remove the effect of the 60 Hz powerline and its second and third harmonics (120 Hz and 180 Hz). Then, two types of features where extracted. First, the LMP, which we computed by low pass filtering the signal with a given cut-off frequency (f_c). We tested different values of f_c, and retained 1.5 Hz or 3.5 Hz, depending on the subject, (see the results and discussion sections). The filtered signal is then integrated over a 50 ms window to obtain the LMP sampled at 20 Hz.

The second type of feature extracted is related to the power in 7 frequency bands, δ (0–5 Hz), θ (5–8 Hz), α (8–12 Hz), $\beta1$ (12–24 Hz), $\beta2$ (24–34 Hz), low gamma band, (34–60 Hz), and high gamma band (HGB) (100–200 Hz). For each band we compute the following:

$$x_i(t_n) = \sum_{t=0}^{\Delta t} b_i^2(t_n + t), \text{ for } i = \delta, \theta, \dots, \text{HGB} \quad (1)$$

where $b_i(t)$ represents the ECoG signal bandpass filtered in the corresponding frequency range of the given band i, e.g. between 0 and 5 Hz when $i = \delta$, and $x_i(t)$ the instantaneous signal power. We set $\Delta t = 50$ ms and $t_{n+1} = t_n + \Delta t$, corresponding to a sampling rate of 20 Hz, the same as for the LMP. Therefore, for each subject, we extracted a total of 8 features, the LMP and the 7 different bands, which were then normalized in a channel-dependent manner to reduce the effect of differences in magnitude. The finger trajectories from the data glove were also normalized and downsampled to 20 Hz in correspondence with the pre-processed ECoG signals.
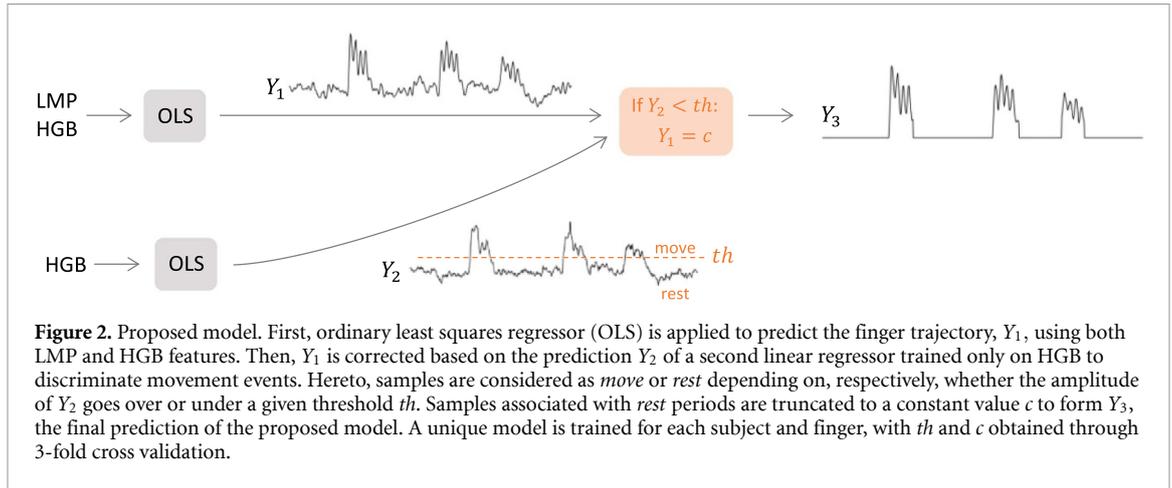
2.4. Linear regression

Linear regression was used to predict finger trajectories from the extracted frequency features. The following linear model was adopted:

$$Y_d = W^T X \quad (2)$$

where Y_d is the finger trajectory vector of n time points and X the tap-delay ECoG data cast into an $m \times n$ matrix, with m the number of taps, set to 20, which defines the one second window of past activity used to make the prediction, times the number of selected channels. The weight vector W, sized

Figure 2. Proposed model. First, ordinary least squares regressor (OLS) is applied to predict the finger trajectory, Y_1, using both LMP and HGB features. Then, Y_1 is corrected based on the prediction Y_2 of a second linear regressor trained only on HGB to discriminate movement events. Hereto, samples are considered as *move* or *rest* depending on, respectively, whether the amplitude of Y_2 goes over or under a given threshold *th*. Samples associated with *rest* periods are truncated to a constant value c to form Y_3, the final prediction of the proposed model. A unique model is trained for each subject and finger, with *th* and c obtained through 3-fold cross validation.

$m \times 1$, was trained for each subject and finger individually following the ordinary least squares (OLS) method [31]:

$$W = \left(\boldsymbol{X}\boldsymbol{X}^{\mathrm{T}}\right)^{-1}\boldsymbol{X}Y_{\mathrm{d}}. \tag{3}$$

In order to ensure the generalization of the results, a 3-fold cross validation approach was adopted. Hereto the ECoG data was equally divided into 3 subgroups, train, validation and test sets, and three decoders were developed in such a way that the subgroups acted once as each type of set. We opted for 3 folds due to the small sample size. The normalizing step mentioned in section 2.3 was performed on each subgroup separately, to avoid information transfer. Forward channel selection was performed by training a linear regressor only on the train set and testing it on the validation set. Here, we started with the channel that gave the best performance and additional channels were added one by one until the performance stopped increasing or until a maximum of 10 channels was reached. Then, using the group of channels previously selected, a new regressor was trained now by merging the train and validation sets. The test set, not involved until now, is then used here to assess the performance of the model.

The Pearson correlation between the predicted trajectories and the actual finger movements, recorded with the data gloves, was used to measure the performance of the linear regression models. The final correlation outcome was obtained by averaging over the correlations of the three folds.

Linear regression models were trained with OLS for each of the 8 spectral features. As all models were subject- and finger-specific, we obtained 45 different performance values per feature. The models were tested on the two movement states defined in figure 1, the movement dynamics and the movement events, as well as on the original finger trajectories. Once the contribution of the individual spectral features was charted, a novel finger decoding model was developed combining only two of the original 8 features: the

feature that better coded for the movement dynamics and the one that better coded for the movement events. The proposed model is shown in figure 2 and explained further.

First, linear regression was applied to predict the finger trajectories using both the LMP and HGB to construct the tap-delay ECoG data matrix ($\boldsymbol{X}$ in equation (1)). We refer to Y_1 as the finger trajectory predicted in this first step. Forward channel selection was performed, as previously explained, but starting from twice the number of channels, as they can be selected per frequency feature (LMP and HGB).

Then, movement events and rest intervals were discriminated based on HGB by applying a threshold *th* to the linear regression result Y_2, this time by training the model using only on HGB features. Equation (4) summarizes how the final finger trajectory prediction Y_3 was obtained:

$$Y_3 = \begin{cases} c, & Y_2 \leqslant th \\ Y_1, & Y_2 > th. \end{cases} \tag{4}$$

The thresholding step is introduced to address the instabilities in the decoding, labelling rest periods by a constant flexion c. The value of *th* and c are subject- and finger-dependent parameters and estimated from the validation set. For this purpose, during forward channel selection, the validation-predicted trajectories associated with the best group of channels are saved. These trajectories are then used in a grid search for the optimal value for *th*, search space $[-0.5:0.01:0.5]$, and c search space $[-1:0.01:0.5]$.

2.5. Feature analysis

The next step was to gain insight into the spatial and temporal contributions of the spectral features that performed best. For the temporal analysis, within the one second window of prior activity, we were interested in which feature holds most information. The weight vectors W of the linear models trained cannot be used for this purpose, as their interpretation can lead to wrong conclusions due to, for instance, the

presence of large weight values assigned to features that help to denoise the signals, but that are otherwise independent of the brain process under study [32]. Therefore, following the procedure laid out in [32], the activation patterns *A* are obtained as follows:

$$A = \boldsymbol{X}^T Y_{\mathrm{d}}. \tag{5}$$

In order to keep the focus on temporal feature contributions, the activation patterns were computed for the best performing electrode, for every subject-finger combination, and averaged over the 3 folds. To obtain an overall measure of the contributions for our analysis, we took the absolute value of the activation patterns.

2.6. Comparison with previous work

To assess the benefit of using distinct frequency features for movement states in trajectory decoding, we compared the proposed model with that developed by Liang and Bougrain in [15]. We choose this study because it also applied linear regression based on OLS, but instead used general frequency features drawn from the full spectrum, i.e. the power in low- (<30 Hz), mid- (30–60 Hz) and high- (>60 Hz) frequency bands. To ensure a fair comparison, we replicated that method, but adapted it to our 3-fold cross validation procedure explained above.

3. Results

3.1. Feature contribution to movement states

Figure 3 shows the contribution of each frequency feature to the decoding of movement dynamics, movement events, and original trajectories. The distribution represented by each boxplot is based on 45 values, coming from the correlation coefficients of 9 subjects and 5 fingers each. The frequency feature yielding the best performance depended on the movement state. Considering movement dynamics, the linear regressor trained with LMP generated the highest correlation coefficients. In contrast, when detecting movement events, HGB was the best performing feature. HGB also outperformed the other features when the models were tested on the original trajectories, suggesting that movement events have a bigger impact than movement dynamics in the overall correlation coefficient.

After confirming the normality of the data with the Kolmogorov–Smirnov test [33], paired *t*-tests were used to assess whether the best performing feature performed significantly better than the others, with low *p*-values indicating statistically significant differences. For the sake of clarity, figure 3 only shows the largest of these *p*-values. Note that, when using a paired test, statistical significance is not always easy to confirm visually from boxplots, so we refer the reader to figure S1, where paired samples are connected to highlight differences across features.
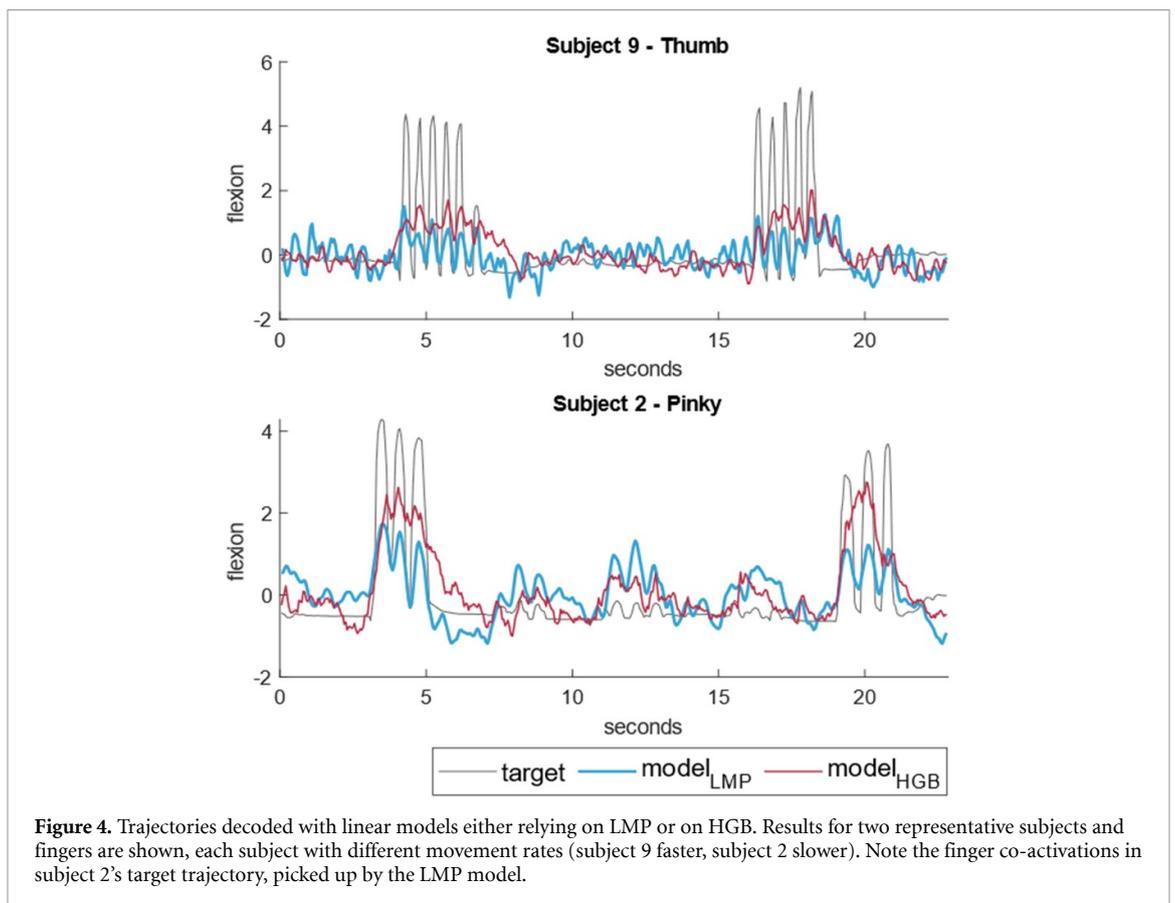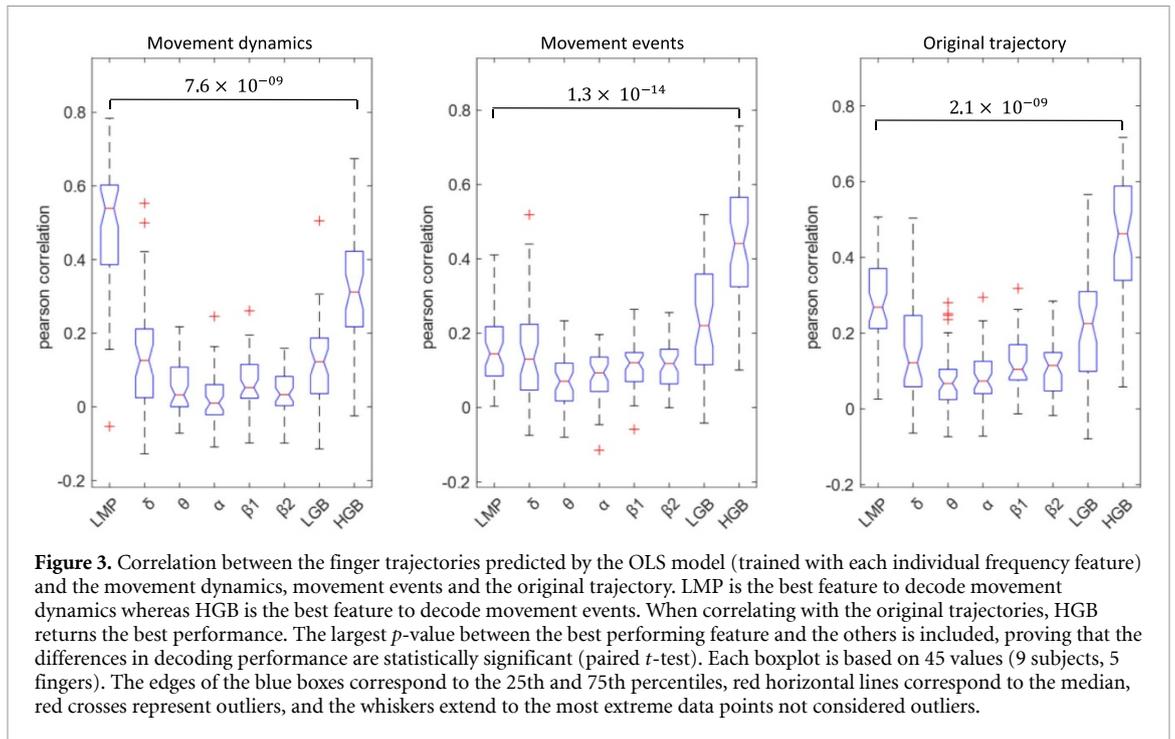
Figure 4 shows, for two representative subjects, the decoded trajectories obtained with the two best performing features: LMP capturing movement dynamics (blue) and HGB movement events (dark red). In addition, figure 4 also illustrates the differences in movement rate between the two subjects, with subject 9 (top) performing, within the 2 s trial, almost twice the number of finger flexions of subject 2 (bottom). Differences in movement rate can be seen across subjects, reflecting the self-paced finger flexions they were asked to perform during the experiments.

The rate of finger movement influences the optimal f_c used in the extraction of LMP from the ECoG signal. For subjects with fast finger movement rates, a low f_c failed to capture the movement dynamics (figure 5(a)). On the other hand, imposing a larger f_c than necessary also had a negative effect in the performance. This can be seen in figure 5(b) where, after reaching an optimum, the performance starts to drop as f_c increases. Values of f_c above 10 Hz are not included in the plot because the performance remains stable after that point. In view of this movement-rate dependency of f_c, we decided to opt for two f_c values: 1.5 Hz and 3.5 Hz for subjects with slow and with fast movement rate, respectively.

The movement rate of each subject was assesed from the derivative of the trajectories recorded with the data glove when looking at the movement dynamics of each finger. The average movement rate per finger is represented in figure 5(c) for every subject, with subjects above the dashed line considered to have a fast movement rate. The reasoning behind opting for a different f_c value for 'fast' and 'slow' moving subjects is shown in figure 5(d), where the power spectra of the data glove-recorded movement dynamics are represented for every subject, here the movement dynamics of every finger were concatenated before generating the spectrum. We observed that the power spectrum of slower finger movements mostly falls below $f_c = 1.5$ Hz and that of faster ones mostly below $f_c = 3.5$ Hz. It is worth emphasizing that the LMP is obtained from the ECoG recordings, not the data glove trajectories, so the low pass filter at f_c is not applied to the data shown in figure 5(d), but to the ECoG data recorded while the finger trajectories are performed.

3.2. Prediction of finger trajectories

The performance of the proposed model, based on the combination of LMP and HGB (section 2.5), is shown in figure 6(a). Results from the method proposed by Liang and Bougrain [15], which is based on general spectral features, are also included. Paired

Figure 3. Correlation between the finger trajectories predicted by the OLS model (trained with each individual frequency feature) and the movement dynamics, movement events and the original trajectory. LMP is the best feature to decode movement dynamics whereas HGB is the best feature to decode movement events. When correlating with the original trajectories, HGB returns the best performance. The largest *p*-value between the best performing feature and the others is included, proving that the differences in decoding performance are statistically significant (paired *t*-test). Each boxplot is based on 45 values (9 subjects, 5 fingers). The edges of the blue boxes correspond to the 25th and 75th percentiles, red horizontal lines correspond to the median, red crosses represent outliers, and the whiskers extend to the most extreme data points not considered outliers.

Figure 4. Trajectories decoded with linear models either relying on LMP or on HGB. Results for two representative subjects and fingers are shown, each subject with different movement rates (subject 9 faster, subject 2 slower). Note the finger co-activations in subject 2's target trajectory, picked up by the LMP model.

t-tests were used to assess statistical significance. Regarding movement dynamics, the proposed model yields a significantly better performance than the model based on HGB only or that of Liang and Bougrain. Similarly, the prediction of the original finger trajectories also enjoys higher correlations, with the proposed model reaching an average coefficient of 0.5, versus 0.45 using the method from Liang and Bougrain. These results suggest that exploiting the distinct role of the LMP and HGB features significantly enhances decoding performance for the movement dynamics and the original finger trajectories.
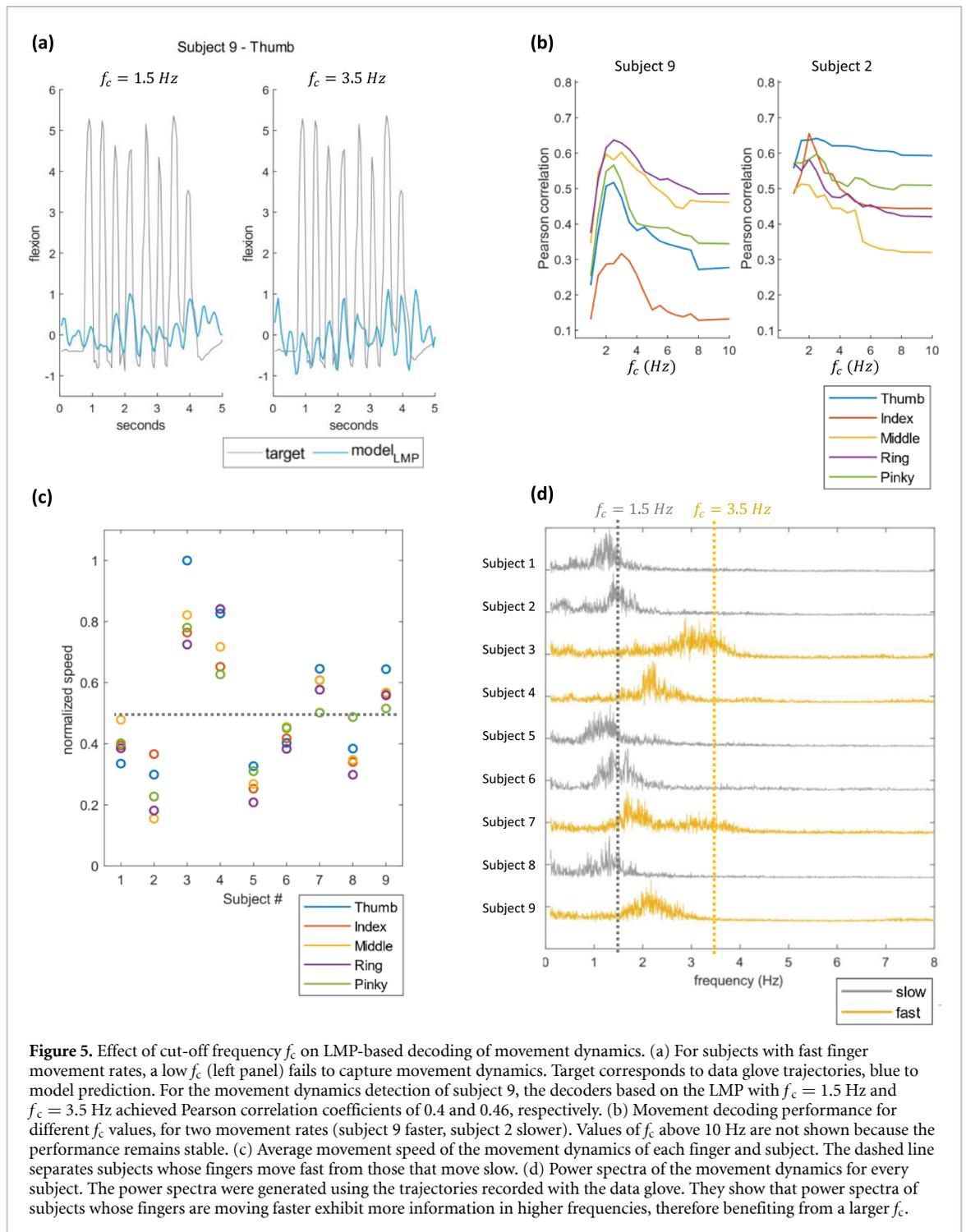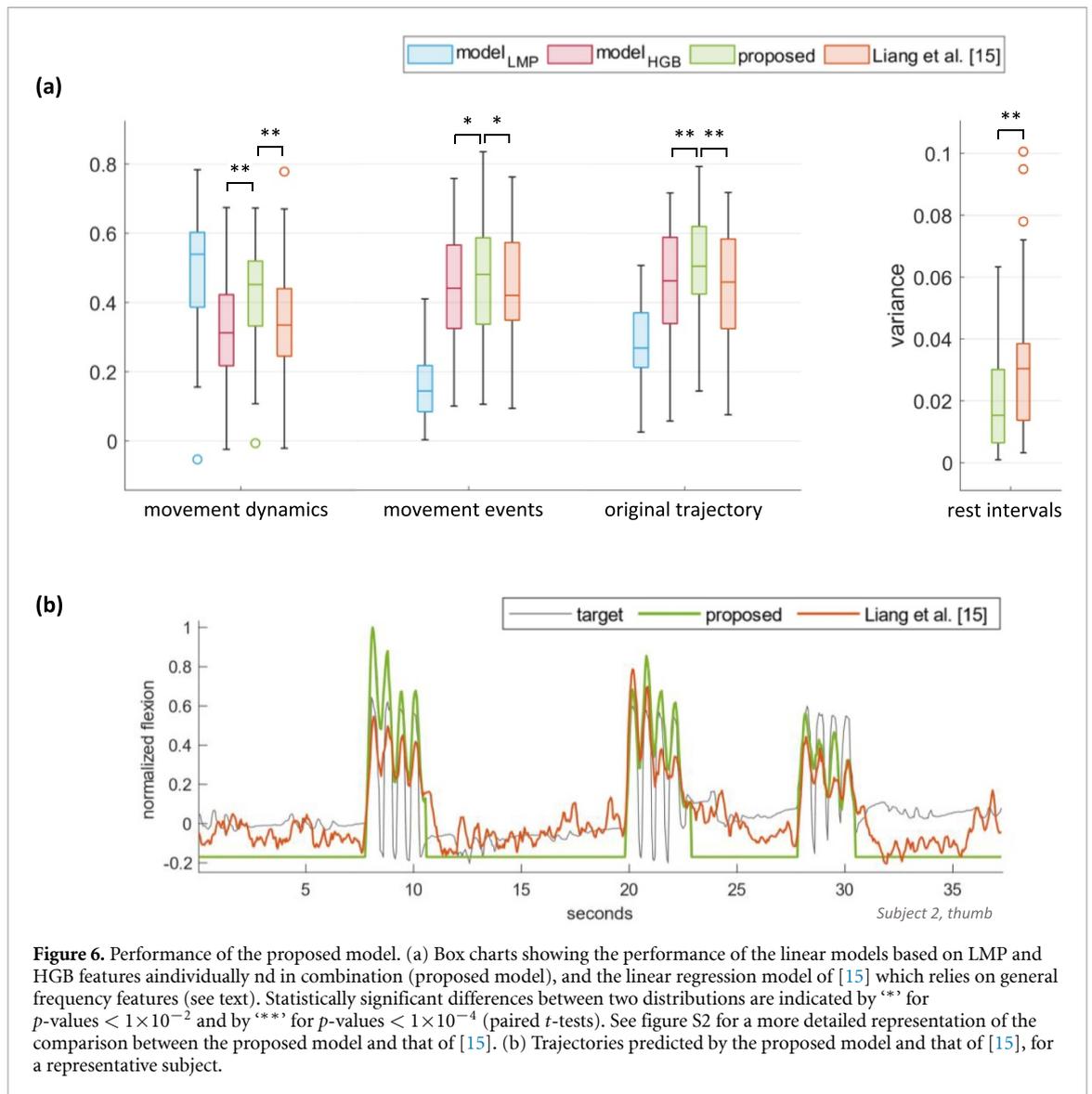
Figure 5. Effect of cut-off frequency f_c on LMP-based decoding of movement dynamics. (a) For subjects with fast finger movement rates, a low f_c (left panel) fails to capture movement dynamics. Target corresponds to data glove trajectories, blue to model prediction. For the movement dynamics detection of subject 9, the decoders based on the LMP with $f_c = 1.5$ Hz and $f_c = 3.5$ Hz achieved Pearson correlation coefficients of 0.4 and 0.46, respectively. (b) Movement decoding performance for different f_c values, for two movement rates (subject 9 faster, subject 2 slower). Values of f_c above 10 Hz are not shown because the performance remains stable. (c) Average movement speed of the movement dynamics of each finger and subject. The dashed line separates subjects whose fingers move fast from those that move slow. (d) Power spectra of the movement dynamics for every subject. The power spectra were generated using the trajectories recorded with the data glove. They show that power spectra of subjects whose fingers are moving faster exhibit more information in higher frequencies, therefore benefiting from a larger f_c.

When it comes to motor BCIs, decoders not only need to accurately predict intended movements but also avoid predicting false attempts. In order to assess the latter, we looked at the variance during rest periods, with lower variances being indicative of more stable performance. Figure 6(a) shows that the proposed model exhibits a significantly lower variance compared to Liang and Bougrain [15] (for more detail on the paired comparison, see figure S2). Note that a zero variance cannot be accomplished because movement event detection through HGB is not perfect. The trajectories predicted by the two models are included in figure 6(b), for a subject 2. The correlation coefficients obtained for individual subjects and fingers are included in table 1 for the 3 subjects of the BCI competition IV dataset, and in table S2 for the 9 subjects of the Stanford dataset. The variances during the rest intervals are included in tables 2 and S3, for the BCI competition IV and Stanford datasets, respectively. For reference's sake, the tables also include the performance obtained following the model of Liang and Bougrain.

Figure 6. Performance of the proposed model. (a) Box charts showing the performance of the linear models based on LMP and HGB features aindividually nd in combination (proposed model), and the linear regression model of [15] which relies on general frequency features (see text). Statistically significant differences between two distributions are indicated by '*' for p-values $< 1 \times 10^{-2}$ and by '**' for p-values $< 1 \times 10^{-4}$ (paired t-tests). See figure S2 for a more detailed representation of the comparison between the proposed model and that of [15]. (b) Trajectories predicted by the proposed model and that of [15], for a representative subject.

3.3. Feature analysis

The results from analysing the spatial and temporal differences between LMP and HGB are summarized in figure 7. The activation patterns of figure 7(a), generated as explained in section 2.5, show the differences in the temporal contribution of both features. The heatmaps were generated for each subject by averaging the activation patterns obtained from each finger; keeping the fingers separate yielded similar results. We observe that HGB mostly contributes in the 250 ms prior to the predicted movement sample (time lag = 0); the LMP, on the other hand, exhibits a more variable contribution across subjects, which can be traced back to the difference in movement rates. Note the occasional double peaks in the activation patterns that correspond to subsequent movement attempts.

Given these temporal differences, the next question is, does the performance of these two features depend on the window length used for regression?

This is plotted in terms of the correlation coefficient in figure 7(b): the performance of HGB steadily increases with window length, but this is not as consistent for LMP, a possible explanation for this effect is presented in the Discussion. For these plots the results from all fingers within a subject were averaged.

Spatial differences between features were assessed by analysing the individual contribution of each channel to the decoding performance. In figure 7(c), we plotted the average number of channels, averaged across subjects, that yielded a performance within 50% of the correlation coefficients reported in 3.2. As expected [23], LMP exhibits a broader spatial distribution than HGB. Furthermore, the difference seems to be greater for the more 'independent' fingers: thumb and index finger. This can be verified also by looking at the distribution of the correlation coefficient over the ECoG grid in figure 7(d), for a representative subject.

Table 1. Comparison of the proposed model with the one reported in [15]. Both methods are based on linear regression. The table lists the Pearson correlation coefficients between the predicted and actual finger trajectories, looking both at the entire trajectory and at the time segments corresponding to movement dynamics (figure 1). The table includes the results from the three subjects originally considered in [15] (see table S1 for the equivalence between the datasets), the results for all subjects are included in table S2.

	Fingers	Liang and Bougrain [15]		Proposed model	
		Movement dynamics	Original trajectory	Movement dynamics	Original trajectory
Subj. 9	Thumb	0.25	0.55	0.39	0.65
	Index	0.57	0.71	0.52	0.73
	Middle	0.29	0.2	0.39	0.21
	Ring	0.4	0.55	0.54	0.61
	Pinky	0.37	0.38	0.4	0.44
	Average	0.38	0.48	0.45	0.53
Subj. 1	Thumb	0.42	0.58	0.46	0.65
	Index	0.49	0.38	0.54	0.45
	Middle	0.15	0.26	0.43	0.5
	Ring	0.53	0.48	0.64	0.57
	Pinky	0.39	0.32	0.46	0.49
	Average	0.4	0.4	0.51	0.53
Subj. 2	Thumb	0.49	0.72	0.50	0.79
	Index	0.38	0.58	0.48	0.6
	Middle	0.49	0.62	0.53	0.59
	Ring	0.27	0.6	0.49	0.65
	Pinky	0.39	0.69	0.47	0.73
	Average	0.41	0.64	0.49	0.67
Average		0.39	0.51	0.48	0.58

Table 2. Comparison of the proposed model with the one reported in [15]. The table lists the variance during rest periods and includes the three subjects considered in [15], the results for all subjects are included in table S3.

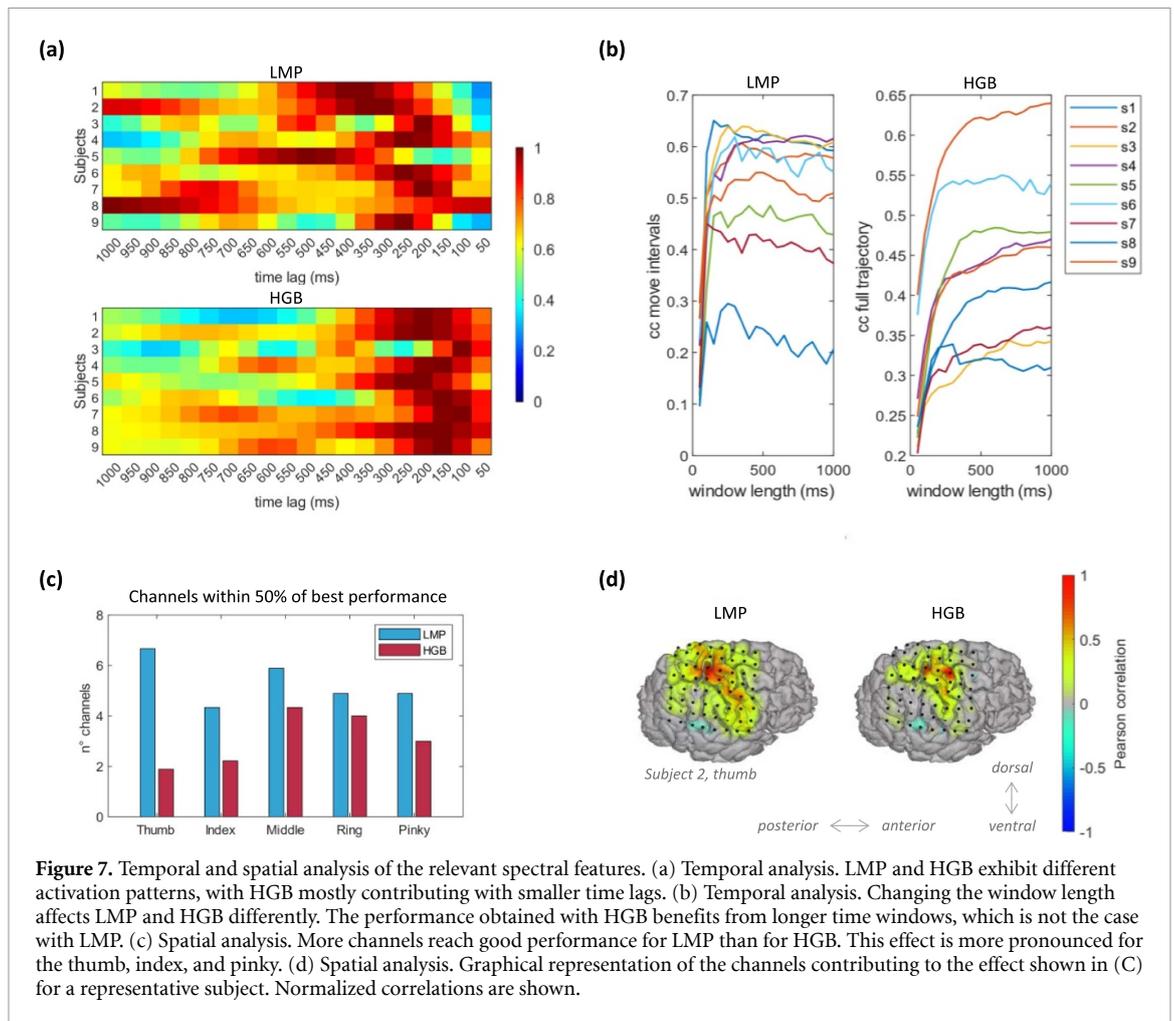|	Fingers	Liang and Bougrain [15]	Proposed model
Subj. 9	Thumb	0.009	0.006
	Index	0.006	0.003
	Middle	0.057	0.053
	Ring	0.03	0.026
	Pinky	0.023	0.01
Subj. 1	Thumb	0.011	0.005
	Index	0.027	0.01
	Middle	0.031	0.013
	Ring	0.022	0.01
	Pinky	0.034	0.005
Subj. 2	Thumb	0.007	0.002
	Index	0.03	0.019
	Middle	0.018	0.029
	Ring	0.052	0.055
	Pinky	0.029	0.02

4. Discussion

In this study, we analysed the contribution of different frequency features to the decoding of finger trajectories from motor ECoG recordings. We showed the differential contribution of LMP and HGB in resolving finger dynamics and detecting finger movement events, which we exploited in a simple decoder that accurately predicts finger trajectories, outperforming comparable prior work where the entire spectrum was used [15], and yielding on par performance compared to recent studies using more complex models [17–19].

LMP signals yielded significantly better performance than other spectral features when decoding finger movement dynamics. Specifically, the superior contribution of the LMP compared to the delta band (figure 3), although they share the same low frequency range, suggests that phase information is key to predict the specific finger flexion and extension patterns. The importance of phase information for motor activity decoded from low frequency rhythms is in agreement with the literature [22, 34].

On the other hand, as shown in figure 4, LMP signals fall short in discriminating finger movement from rest or when a given finger was moved involuntarily due to co-activations caused by other fingers. The effect of co-activations can be seen in the bottom graph of this figure, where the trajectory of the pinky finger shows small fluctuations between cued finger movements, corresponding to index and middle finger flexions. A possible explanation could be that LMP activity extends over the entire 'hand knob' cortical region, making it hard to resolve the activity patterns of individual fingers (figure 7(d)). In addition, low frequency rhythms have also been linked to subcortical areas [23], which might not be

Figure 7. Temporal and spatial analysis of the relevant spectral features. (a) Temporal analysis. LMP and HGB exhibit different activation patterns, with HGB mostly contributing with smaller time lags. (b) Temporal analysis. Changing the window length affects LMP and HGB differently. The performance obtained with HGB benefits from longer time windows, which is not the case with LMP. (c) Spatial analysis. More channels reach good performance for LMP than for HGB. This effect is more pronounced for the thumb, index, and pinky. (d) Spatial analysis. Graphical representation of the channels contributing to the effect shown in (C) for a representative subject. Normalized correlations are shown.

well gauged as ECoG grids are placed on the cortical convexity.

In order to extract LMP signals from ECoG recordings, a wide range of upper cut-off frequencies of the low pass filter have been proposed, going from 40 Hz in [34], to 3.6 Hz in [35], and down to 1 Hz in [27], or even by applying a moving average window of various lengths on the unfiltered recordings [18, 36, 37]. In this study, we showed that, when a moving average window of 50 ms is applied, including a prior low pass filtering epoch increases the performance of finger movement decoders. Furthermore, this increase in performance is maximal when the cut-off frequency of the filter accounts for the finger movement rate (figure 5(b)). To ensure that the reported LMP performance were not originating from artefactual movements of electrode leads, we looked at how the performance varies across channels (figures 7(d) and S3). Good performances were limited to a few channels of the sensorimotor cortex, suggesting neural signals as the driver of these performances, not motor artefacts, as the latter would have affected all channels equally.

For the prediction of movement events, where 'event' refers to the time interval during which subjects were voluntarily moving a given finger, HGB activity outperformed all other frequency features. HGB has previously been linked to motor behaviour and is believed to represent localized spiking activity [25, 38]. This localization shows up in the ECoG grid as distinct cortical patterns per finger, patterns that can be differentiated by the decoder [39, 40]. In addition, our results show the relation between the spreading of HGB activity and the level of independence of the corresponding finger [41] (figure 7(c)) with fewer channels contributing to the decoding of the more 'independent' fingers—thumb and index finger–, more channels to the least independent ones—middle and ring finger–, and an intermediate level of independence for the pinky, in accordance with the findings reported in [41].

In contrast, when it comes to movement dynamics of finger flexion and extension, HGB activity yields lower decoding performance. Previous work has shown a significant overlap in the cortical representation of finger flexion and extension [9], which could prevent their differentiation.

The distinct properties of HGB allow for more stable predictions of finger trajectories, reducing the fluctuations between volitional attempts by applying, for instance, a simple threshold (figure 2). In addition, these results suggest that HGB would also be the best feature to classify finger movement from rest, in agreement with the literature where the higher frequencies were found to contribute most to classifier performance [10–12]. We tried to subdivide the HGB frequency range in two different bands, (60–100 Hz) and (>100 Hz), but got similar results from both bands, suggesting the presence of redundant activity.

Regarding the temporal activation patterns (figure 7(a)), LMP holds information in a broader window of prior activity, whereas for HGB the most recent samples are the most relevant ones. This difference in activation patterns is linked to the finger movement rate. LMP captures, within the one second window, the dynamics corresponding to past flexion/extension activity, while HGB captures this to a much lesser extent, holding instead information related to the overall prior movement of the finger. Surprisingly, when different window lengths were used to build the decoders for each feature (figure 7(b)), LMP was less affected by shorter windows than HGB. This suggests that the prior flexions/extensions represented in the LMP do not provide extra information to the decoders, but, instead, act as an interference that slightly lowers decoding performance.

Finally, the datasets used in this study come from subjects performing finger flexions in a repetitive manner. Prior research has been done regarding differences between single and repetitive movements both for ECoG [22] and EEG [42]. Specifically, a decrease in HGB activity after the start of repetitive movement was reported in [22]. We accounted for this effect by checking whether HGB performance was better at the beginning of the movement compared to the end, but found no conclusive results.

5. Conclusion

In this work we showed the complementary contribution of two ECoG frequency features to finger movement decoding, with HGB distinguishing movement events from rest and LMP coding for movement dynamics. We exploited the distinct role of these features to build a simple decoder, obtaining performances on par with the state of the art that relies on more complex models. Our results also demonstrate the relationship between LMP performance and finger movement rate, with the rate defining the optimal cut-off frequency of the low pass filter. In addition, differences in the behaviour of LMP and HGB also arose when we looked at their spatial coverage and when we varied the window length used in the decoders, with HGB being more affected by shorter windows.

ORCID iDs

Eva Calvo Merino ⬤ https://orcid.org/0000-0002-8782-3856
A Faes ⬤ https://orcid.org/0000-0002-1637-255X
M M Van Hulle ⬤ https://orcid.org/0000-0003-1060-7044

References

[1] WHO 2013 Spinal cord injury (available at: www.who.int/news-room/fact-sheets/detail/spinal-cord-injury) (Accessed 12 May 2023)

[2] Bouton C E *et al* 2016 Restoring cortical control of functional movement in a human with quadriplegia *Nature* **533** 247–50

[3] Ajiboye A B *et al* 2017 Restoration of reaching and grasping movements through brain-controlled muscle stimulation in a person with tetraplegia: a proof-of-concept demonstration *Lancet* **389** 1821–30

[4] Collinger J L, Wodlinger B, Downey J E, Wang W, Tyler-Kabara E C, Weber D J, McMorland A J, Velliste M, Boninger M L and Schwartz A B 2013 High-performance neuroprosthetic control by an individual with tetraplegia *Lancet* **381** 557–64

[5] Wodlinger B, Downey J E, Tyler-Kabara E C, Schwartz A B, Boninger M L and Collinger J L 2015 Ten-dimensional anthropomorphic arm control in a human brain-machine interface: difficulties, solutions, and limitations *J. Neural Eng.* **12** 1

[6] Benabid A L *et al* 2019 An exoskeleton controlled by an epidural wireless brain–machine interface in a tetraplegic patient: a proof-of-concept demonstration *Lancet Neurol.* **18** 1112–22

[7] Willett F R, Avansino D T, Hochberg L R, Henderson J M and Shenoy K V 2021 High-performance brain-to-text communication via handwriting *Nature* **593** 249–54

[8] Sobinov A R and Bensmaia S J 2021 The neural mechanisms of manual dexterity *Nat. Rev. Neurosci.* **22** 741–57

[9] Schellekens W, Petridou N and Ramsey N F 2018 Detailed somatotopy in primary motor and somatosensory cortex revealed by Gaussian population receptive fields *NeuroImage* **179** 337–47

[10] Onaran I, Ince N F and Cetin A E 2011 Classification of multichannel ECoG related to individual finger movements with redundant spatial projections *Proc. Annual Int. Conf.*

IEEE Engineering in Medicine and Biology Society, EMBS (*Boston, Massachusetts USA*) pp 5424–7

[11] Jiang T, Jiang T, Wang T, Mei S, Liu Q, Li Y, Wang X, Prabhu S, Sha Z and Ince N F 2017 Characterization and decoding the spatial patterns of hand extension/flexion using high-density ECoG *IEEE Trans. Neural Syst. Rehabil. Eng.* **25** 370–9

[12] Delgado Saa J F, De Pesters A and Cetin M 2016 Asynchronous decoding of finger movements from ECoG signals using long-range dependencies conditional random fields *J. Neural Eng.* **13** 3

[13] Yao L and Shoaran M 2019 Enhanced classification of individual finger movements with ECoG *Conf. Record Asilomar Conf. Signals System Computer* vol 2019 pp 2063–6

[14] Miller K J and Schalk G 2008 Prediction of finger flexion 4 th brain-computer interface data competition *New York* pp 5–6 (available at: www.bbci.de/competition/iv/desc_4.pdf)

[15] Liang N and Bougrain L 2012 Decoding finger flexion from band-specific ecog signals in humans *Front. Neurosci.* **6** 1–6

[16] Tangermann M *et al* 2012 Review of the BCI competition IV *Front. Neurosci.* **6** 1–31

[17] Xie Z, Schwartz O and Prasad A 2018 Decoding of finger trajectory from ECoG using deep learning *J. Neural Eng.* **15** 036009

[18] Yao L, Zhu B and Shoaran M 2022 Fast and accurate decoding of finger movements from ECoG through Riemannian features and modern machine learning techniques *J. Neural Eng.* **19** 1

[19] Faes A, Camarrone F and Hulle M M V 2022 Single finger trajectory prediction from intracranial brain activity using block-term tensor regression with fast and automatic component extraction *IEEE Trans. Neural Netw. Learn. Syst.* 1–12

[20] Volkova K, Lebedev M A, Kaplan A and Ossadtchi A 2019 Decoding movement from electrocorticographic activity: a review *Front. Neuroinform.* **13** 1–20

[21] Schalk G and Leuthardt E C 2011 Brain-computer interfaces using electrocorticographic signals *IEEE Rev. Biomed. Eng.* **4** 140–54

[22] Miller K J, Hermes D, Honey C J, Hebb A O, Ramsey N F, Knight R T, Ojemann J G and Fetz E E 2012 Human motor cortical activity is selectively phase-entrained on underlying rhythms *PLoS Comput. Biol.* **8** 9

[23] Opri E, Cernera S, Okun M S, Foote K D and Gunduz A 2019 The functional role of thalamocortical coupling in the human motor network *J. Neurosci.* **39** 8124–34

[24] Jiang T *et al* 2015 Local spatial correlation analysis of hand flexion/extension using intraoperative high-density ECoG *Proc. Annual Int. Conf. IEEE Engineering in Medicine and Biology Society, EMBS* vol 2015 pp 6190–3

[25] Assem M *et al* 2023 High gamma activity distinguishes frontal cognitive control regions from adjacent cortical networks *Cortex* **159** 286–98

[26] Gunduz A, Brunner P, Sharma M, Leuthardt E C, Ritaccio A L, Pesaran B and Schalk G 2016 Differential roles of high gamma and local motor potentials for movement preparation and execution *Brain Comput. Interfaces* **3** 88–102

[27] Camarrone F, Branco M P, Ramsey N F and Van Hulle M M 2021 Accurate offline asynchronous detection of individual finger movement from intracranial brain signals using a novel multiway approach *IEEE Trans. Biomed. Eng.* **68** 2176–87

[28] Lega B, Burke J, Jacobs J and Kahana M J 2016 Slow-theta-to-gamma phase-amplitude coupling in human hippocampus supports the formation of new episodic memories *Cereb. Cortex* **26** 268–78

[29] Miller K J 2019 A library of human electrocorticographic data and analyses *Nat. Hum. Behav.* **3** 1225–35

[30] Lang C E and Schieber M H 2004 Human finger independence: limitations due to passive mechanical coupling versus active neuromuscular control *J. Neurophysiol.* **92** 2802–10

[31] Amemiya T 1977 Some theorems in the linear probability model *Int. Econ. Rev.* **18** 645

[32] Haufe S, Meinecke F, Görgen K, Dähne S, Haynes J-D, Blankertz B and Bießmann F 2014 On the interpretation of weight vectors of linear models in multivariate neuroimaging *NeuroImage* **87** 96–110

[33] Massey F J Jr 1951 The Kolmogorov-Smirnov test for goodness of fit *J. Am. Stat. Assoc.* **46** 68–78

[34] Delgado Saa J, Christen A, Martin S, Pasley B N, Knight R T and Giraud A-L 2020 Using Coherence-based spectro-spatial filters for stimulus features prediction from electro-corticographic recordings *Sci. Rep.* **10** 1–14

[35] Bundy D T, Pahwa M, Szrama N and Leuthardt E C 2016 Decoding three-dimensional reaching movements using electrocorticographic signals in humans *J. Neural Eng.* **13** 2

[36] Benz H L, Zhang H, Bezerianos A, Acharya S, Crone N E, Zheng X and Thakor N V 2012 Connectivity analysis as a novel approach to motor decoding for prosthesis control *IEEE Trans. Neural Syst. Rehabil. Eng.* **20** 143–52

[37] Flint R D *et al* 2014 Extracting kinetic information from human motor cortical signals *NeuroImage* **101** 695–703

[38] Unterweger J, Seeber M, Zanos S, Ojemann J G and Scherer R 2020 ECoG beta suppression and modulation during finger extension and flexion *Front. Neurosci.* **14** 1–10

[39] Wang W *et al* 2009 Human motor cortical activity recorded with micro-ECoG electrodes, during individual finger movements *Proc. 31st Annual Int. Conf. IEEE Engineering in Medicine and Biology Society: Engineering the Future of Biomedicine, EMBC 2009* pp 586–9

[40] Siero J C W, Hermes D, Hoogduin H, Luijten P R, Ramsey N F and Petridou N 2014 BOLD matches neuronal activity at the mm scale: a combined 7T fMRI and ECoG study in human sensorimotor cortex *NeuroImage* **101** 177–84

[41] Hager-Ross C and Schieber M H 2000 Quantifying the independence of human finger movements: comparisons of digits, hands, and movement frequencies *J. Neurosci.* **20** 8542–50

[42] Hervault M, Zanone P-G, Buisson J-C and Huys R 2021 Cortical sensorimotor activity in the execution and suppression of discrete and rhythmic movements *Sci. Rep.* **11** 1–15